Beam Divergence with Harmonic Gyroresonance in Focusing Wiggler and Axial Field

K. Sakamoto, T. Kobayashi,[a] Y. Kishimoto, S. Kawasaki,[a] S. Musyoki, A. Watanabe, M. Takahashi,[a] H. Ishizuka,[b] and M. Shiho

Department of Fusion Engineering Research, Japan Atomic Energy Research Institute, Naka-machi, Ibaraki, 311-01, Japan

(Received 3 August 1992)

The transport of a relativistic electron beam was studied experimentally and numerically in a magnetic field configuration which consists of a focusing wiggler as well as an additional axial guide field. A new beam divergence was found for the lower side of the magnetoresonance. It was identified as due to the effect of the second harmonic mode of the cyclotron frequency in the resonance, determined by $n\Omega_{\parallel}=k_w v_{\parallel}$ for $n=2$. The harmonic resonance was detected for the planar wiggler first, and it could appear also for the helical one.

PACS numbers: 41.75.Ht, 41.85.Ja, 52.75.Ms

Successful operation of a Raman free electron laser (FEL) using a relativistic electron beam (REB) has been reported for both planar and helical wiggler configurations [1–4]. To obtain a high-power performance of the FEL, a stable transport of the beam in the wiggler is one of the key issues. The introduction of an axial uniform guide field superimposed on the wiggler is usually required to keep the orbital stability in the transport, while it will involve some other complex features like the magnetoresonance between the cyclotron motions and the wiggling of the electrons [5]. It is well recognized that the beam diverges and spills out when the electron cyclotron frequency $\Omega_{\parallel}$ in the guide field B_g approaches the wiggling frequency $K_w v_{\parallel}$, where k_w is a wiggler wave number, $\Omega_{\parallel}=eB_g/\gamma_0 m_e$, $\gamma_0=\{1-(\mathbf{v}^2/c^2)\}^{-1/2}$, $\mathbf{v}$ and c are electron and light speed, respectively, and the suffix $\parallel$ indicates axial components [6].

In this Letter we describe an experimental and numerical study on the transport of a REB ($E_b\sim 0.8$ MeV and $I_b\sim 300$ A) through a combination of a focusing type planar wiggler [7] and an axial field: We retain a relatively low additional B_g to control the beam dynamics at the entrance of the wiggler and the FEL performance. We found a new type of beam loss at an axial field far lower than the value of B_g corresponding to the fundamental magnetoresonance $\Omega_{\parallel}=k_w v_{\parallel}$; e.g., the loss is in the parameter region of the so-called group I. Therefore it clearly differs from the "harmonic" gyroresonance which was predicted to occur in group II at $\bar{\Omega}_{\parallel}=nk_w v_{\parallel}$ (n an integer) by Chu and Lin [8], where $\bar{\Omega}_{\parallel}$ is a time-averaged cyclotron frequency in $B_{\parallel}$. We need another explanation for the new resonance. We made an analytical study and a numerical simulation on the resonance and its effect on the beam transport through the wiggler. We carried out a similar numerical study for the case of a helical wiggler and the result suggests we will also have the same kind of resonance and beam degradation. The magnetic field in a planar focusing wiggler with a uniform field $B_g\mathbf{e}_z$ is given by

$$\mathbf{B}(\mathbf{r})=B_w\{\cos(k_w z)[\sinh(k_x x)\sinh(k_y y)\mathbf{e}_x+\cosh(k_x x)\cosh(k_y y)\mathbf{e}_y]-\sqrt{2}\sin(k_w z)\cosh(k_x x)\sinh(k_y y)\mathbf{e}_z\}+B_g\mathbf{e}_z\,, \tag{1}$$

where $k_x=k_y=k_w/\sqrt{2}$ and the wiggler axis is in the z direction, and x and y are the horizontal and vertical coordinates transverse to the beam propagation [9]. The field is sufficiently approximated near the axis by

$$\mathbf{B}(\mathbf{r})\sim B_w[1+(k_x x)^2]\cos(k_w z)\mathbf{e}_y+B_g\mathbf{e}_z \quad \text{for } y\sim 0\,. \tag{2}$$

The transverse motion of the electrons in the wiggler is given by

$$\frac{d\mathbf{v}_{\perp}}{dt}=\bar{\Omega}_{\parallel}\mathbf{v}_{\perp}\times\mathbf{e}_z+F(x)\cos(\omega t)\mathbf{e}_x\,; \tag{3}$$

here $\mathbf{v}_{\perp}$ is the vertical velocity component, $\omega t=k_w\bar{v}_{\parallel}t$, and $\bar{v}_{\parallel}$ is a time-averaged axial electron velocity. The first term represents cyclotron motion of the electron in B_g, and $F(x)$ in the second is a force applied on the electron by the wiggler,

$$F(x)\sim\bar{v}_{\parallel}\Omega_w[1+(k_x x)^2]\,; \tag{4}$$

here, $\Omega_w=eB_w/\gamma_0 m_e$. Since $\bar{v}_{\parallel}\sim$const and $(k_x x)^2\ll 1$, the first-order solution of the vertical velocity of the electron is composed of two terms:

$$v_x=v_g\cos(\bar{\Omega}_{\parallel}t+\phi)+\alpha\sin(\omega t)\,, \tag{5}$$

where

$$\alpha=-\omega F(x_0)/(\bar{\Omega}_{\parallel}^2-\omega^2)\,, \tag{6}$$

and v_g and ϕ are the velocity and the phase of the cyclotron motion, respectively. x_0 is the guiding center of the electrons, free from the cyclotron motion and focusing. Equation (5) is integrated to yield

$$x=x_0+\Delta x=x_0+(v_g/\bar{\Omega}_{\parallel})\sin(\bar{\Omega}_{\parallel}t+\phi)-(\alpha/\omega)\cos(\omega t)\,, \tag{7}$$

which reveals that there is a magnetoresonance at $\bar{\Omega}_{\parallel}\pm\omega\approx 0$ through α. The second-order solution is obtained by a successive iteration. Putting Eq. (7) into (4), we obtain

$$F(x)\sim F(x_0)+2F(0)k_x^2 x_0\Delta x+F(0)(k_x\Delta x)^2\,. \tag{8}$$

The first term in Eq. (8) gives the solutions Eq. (5) and Eq. (7), and from the next term the second-order solution becomes

$$v_{x,2}=F(0)k_x^2x_0\{v_g\cos[(\bar{\Omega}_\parallel+\omega)t+\phi]/[\bar{\Omega}_\parallel(2\bar{\Omega}_\parallel+\omega)] + v_g\cos[(\bar{\Omega}_\parallel-\omega)t+\phi]/[\bar{\Omega}_\parallel(2\bar{\Omega}_\parallel-\omega)] + a\sin 2\omega t/[(2\omega-\bar{\Omega}_\parallel)(2\omega+\bar{\Omega}_\parallel)]\}. \quad (9)$$

When the conditions of the harmonic resonances

$$2\bar{\Omega}_\parallel\pm\omega\approx 0, \quad \bar{\Omega}_\parallel\pm 2\omega\approx 0$$

are satisfied, the wiggling amplitude will grow and then the larger transversal velocity will be introduced. Similarly, from the third term there comes the harmonic resonance conditions,

$$3\bar{\Omega}_\parallel\pm\omega\approx 0, \quad \bar{\Omega}_\parallel\pm 3\omega\approx 0.$$

If we proceed with the iteration further, the general conditions for all higher harmonic resonances are obtained. These include the results of Chu and Lin, and also show the existence of a new harmonic resonance. The wiggler field B_w contributes to the longitudinal field in the first order through its z component for $y\sim 0$,

$$B_\parallel=-B_w\sqrt{2}\sin(\omega t)[1+(k_xx_0)^2](k_yy)+B_g, \quad (10)$$

where y should be evaluated at the electron position,

$$y\sim(a\bar{\Omega}_\parallel/\omega^2)\sin\omega t. \quad (11)$$

Equations (10) and (11) give the time-averaged axial field $\bar{B}_\parallel$ and cyclotron frequency $\bar{\Omega}_\parallel$ experienced by electrons as

$$\bar{B}_\parallel\sim -B_w[1+(k_xx_0)^2]\frac{k_ya\bar{\Omega}_\parallel}{\sqrt{2}\omega^2}+B_g, \quad (12)$$

which is rewritten for the cyclotron frequency:

$$\bar{\Omega}_\parallel\sim -[1+(k_xx_0)^2]^2\frac{\Omega_w^2\bar{\Omega}_\parallel}{2(\bar{\Omega}_\parallel^2-\omega^2)}+\Omega_\parallel. \quad (13)$$

As $\bar{\Omega}_\parallel$ is a function of Ω_w, the field of magnetoresonance shifts depending on B_w. The second harmonic of the magnetoresonance typically will occur toward a lower field as B_w increases at

$$\Omega_\parallel\sim\frac{\omega}{2}-\frac{\Omega_w^2}{3\omega}[1+(k_xx_0)^2]^2, \quad (14)$$

which is obtained substituting the resonance condition $2\bar{\Omega}_\parallel\sim\omega$ into Eq. (13). To investigate the beam transport in the magnetic configuration, the orbit of the electrons was traced numerically using the field represented by Eq. (1). We neglect simply the beam space charge and other collective effects on individual beam particles assuming the beam intensity to be relatively low. The equation of motion used in the following calculation is

$$\gamma_0mv_\parallel\frac{d\mathbf{v}}{dz}=e\mathbf{v}\times\mathbf{B}, \quad (15)$$

and is solved numerically by the Runge-Kutta method. Here, γ_0 is constant. In the simulation, 100 electrons are traced, assuming equal distribution initially in both the radial and angular directions. The wiggler period λ_w, and the radii of the drift tube and the beam are 45, 10, and 7.5 mm, respectively. Figures 1(a), 1(b), and 1(c) are the results of the simulation for $B_w=0.6$, 1.0, and 1.4 kG, respectively, showing B_g dependence of the beam transport ratio η defined as the beam at the 50th period of the wiggler, normalized with the initial value. The wiggler is tapered in the first five sections and the adiabatic field variation therein is taken into account. The particle energy in the beam is 800 keV. When B_g becomes high, η decreases finally to zero. This is attributed to the fundamental magnetoresonance, which separates the regions of groups I and II. At B_g lower than the fundamental resonance ($\sim$2.5 kG, when B_w is low), a dip appears in η and the beam intensity suffers about (30–50)% attenuation. The cause of the intensity reduction is not expected from

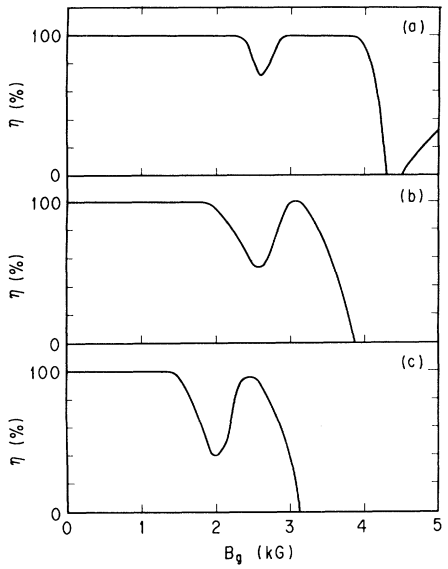

FIG. 1. The dependence of the beam transport ratio η on the axial field B_g for a planar wiggler at $L=50\lambda_w$. $E_b=800$ keV, $\lambda_w=45$ mm. (a) $B_w=0.6$ kG, (b) 1.0 kG, and (c) 1.4 kG.

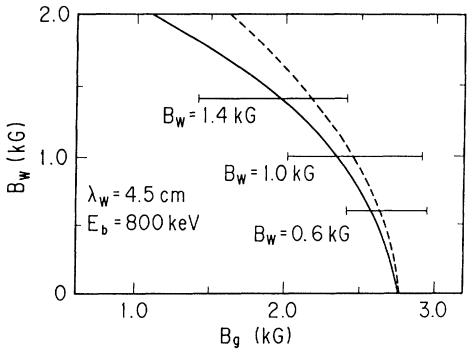

FIG. 2. The region of $B_\parallel$ where the dip appeared on the beam transport ratio of Fig. 1 for $B_w=0.6$, 1.0, and 1.4 kG. The solid and dashed curves are the analytical resonance conditions [Eq. (14)] for $k_xx_0=0.71$ and 0.5, respectively.

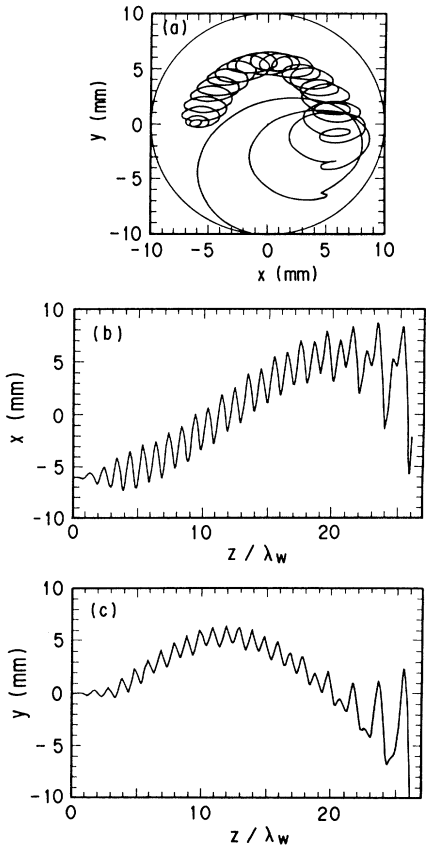

FIG. 3. Trajectory of the electron at $B_w=1.0$ kG, $B_g=2.5$ kG, $E_b=800$ keV, and $\lambda_w=45$ mm. Initial position is $x=-6.0$ mm, $y=0$ mm. (a) Projectional view (on the x-y plane). (b) x position vs axial distance z/λ_w. (c) y position vs axial distance z/λ_w.

the theories presented so far. In Fig. 2, the regions where the dips appeared are plotted in a B_w-B_g diagram for $B_w=0.6$, 1.0, and 1.4 kG. On the other hand, the solid and dashed lines indicate the analytical values of the resonance field of the second harmonic, which is derived from Eq. (14), for $k_x x_0=0.71$ and 0.5, respectively (corresponding to guiding centers $x_0=7.1$ and 5.0 mm, respectively). The figure clearly shows that the dips are attributed to the second harmonic resonance. The trajectories of the electron with the initial positions $(x,y)=(6.0,0)$ mm are shown in Figs. 3(a)–3(c) as the projections of x-y, x-z, and y-z planes. Figure 3(a) gives the transversal drift due to the inhomogeneous field of the wiggler, which starts in the y direction at first, and then the guiding center of the cyclotron motion begins to rotate clockwise around the axis as the result of the betatron oscillation. The particle eventually gains a sufficiently large transversal energy and is finally intercepted by the wall. The period of the electron quiver motion coincides with λ_w initially, while the amplitude is gradually modulated with the period $2\lambda_w$ [Figs. 3(b) and 3(c)]. After reaching $z\sim 20\lambda_w$, the quiver motion of the $2\lambda_w$ period dominates and comes with a rapid growth of the cyclotron gyration, which corresponds to the second harmonic resonance.

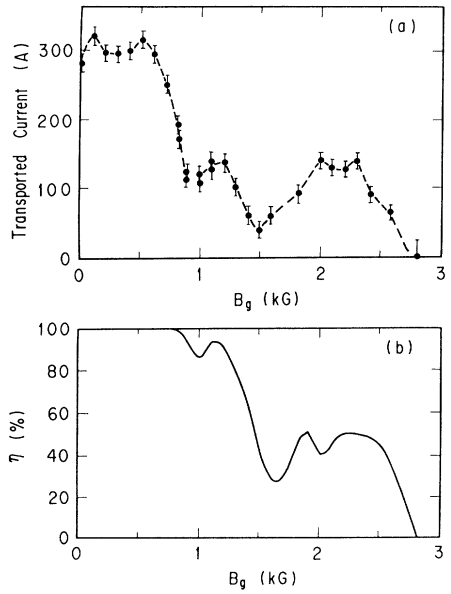

FIG. 4. (a) Experimental result of the axial field dependence on the transported beam at the end of the wigger: $L=33\lambda_w$. $E_b\sim 800$ keV, $B_w=1.8$ kG, and $\lambda_w=45$ mm. (b) Simulation result of the axial field dependence on the beam transport ratio η. The parameters of the simulation are the same as the experiment.

We carried out an experiment of the beam transport in a focusing planar wiggler configuration, where B_w is provided with an array of permanent magnets and B_g with a solenoid. The details of the experiment were reported elsewhere previously [10], and a brief description will be given. The pole face of the magnets has a parabolic

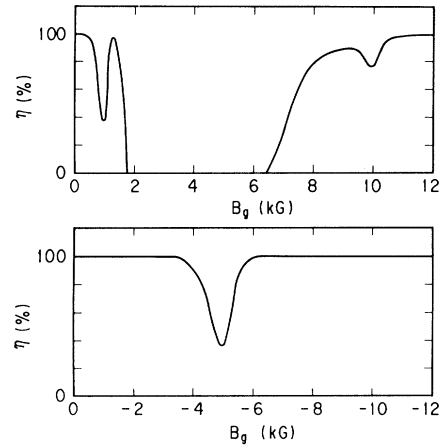

FIG. 5. The dependence of the axial field B_g on η for a helical wiggler at $L=50\lambda_w$. $B_w=1.3$ kG, $E_b=800$ keV, $\lambda_w=45$ mm.

shape to give the field of Eq. (1). The magnets are made of Nd-Fe-B to give $B_w \sim 1.8$ kG and have 33 periods with pitch length of 45 mm, including 5 periods of the entrance adiabatic tapered section. An intense moderately relativistic electron beam ($E_b \gtrsim 800$ keV) is generated by four-stage inductive accelerating modules and transmitted into a drift tube of 22.4 mm diameter through the wiggler. The dependence of the beam transport on B_g with a fixed B_w is measured at the end of the wiggler ($L \sim 1.5$ m) and compared with the simulation. Typical examples are shown in Figs. 4(a) and 4(b). These two figures agree well in revealing common features: (1) Above 2.8 kG, the beam ceases to propagate due to the fundamental resonance; (2) at $B_g \sim 1.6$ kG there is a dip down to $\sim 20\%$; (3) under 0.6 kG, good beam transport is obtained; and (4) at $B_g \sim 1.0$ and 2.0 kG subsidiary small dips seem to appear. It is expected from Fig. 2 that the second harmonic resonance occurs at around $B_g \sim 1.6$ kG, which corresponds to the experimental result. Therefore, the dip observed experimentally at $B_g \sim 1.6$ kG is identified to be due to the second harmonic. The small dips at $B_g = 1.0$ and 2.0 may be caused by the harmonic of $3\bar{\Omega}_\parallel \pm \omega \approx 0$ and $3\bar{\Omega}_\parallel \pm 2\omega \approx 0$, respectively.

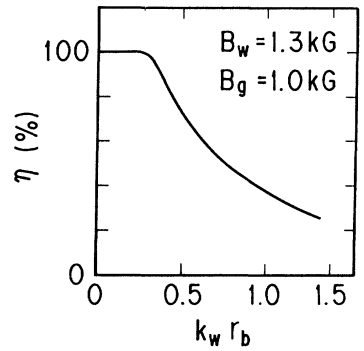

FIG. 6. The dependence of the initial beam radius r_b on the beam transport ratio for a helical wiggler at $B_g = 1.0$ kG with the same parameters of Fig. 5.

We also studied numerically the beam transport in a helical wiggler. The helical wiggler has an intrinsic focusing which would limit the transversal drift of the particles due to the field gradient. Figure 5 gives the dependence of the beam transport on B_g with the parameters $B_w = 1.3$ kG, $E_b = 800$ keV, and $\lambda_w = 45$ mm. The helical field B_w is assumed as

$$\mathbf{B}_w(\mathbf{x}) = 2B_w[I_1'(k_w r)\cos(\phi - k_w z)\mathbf{e}_r - I_1(k_w r)/(k_w r)\sin(\phi - k_w z)\mathbf{e}_\phi + I_1(k_w r)\sin(\phi - k_w z)\mathbf{e}_z] + B_g \mathbf{e}_z , \quad (16)$$

where I_1 and I_1' are the modified Bessel function and its derivative, respectively [11]. The radii of the beam and the drift tube are assumed to be 7.5 and 10 mm, respectively. The upper figure is for the usual direction of B_g and the lower for the reversed direction. A dip due to the second harmonic is found at $B_g \sim 1.0$ kG. Another small dip around $B_g \sim 10$ kG corresponds to the resonance due to the spatial harmonic of the wiggler, $\bar{\Omega}_\parallel \sim 2k_w v_\parallel$. A deep dip appearing at $B_g \sim -5$ kG corresponds to the resonance, $-\bar{\Omega}_\parallel \sim k_w v_\parallel$ [8]. The beam transport near these resonances, however, is subject to the beam radius. Figure 6 shows the dependence of the transported current on the initial beam radius at $B_g = 1.0$ kG, where the dip due to the second harmonic resonance appeared. The simulation indicates that when the initial radius of the beam r_b is reduced to $r_b \sim 0.3/k_w (\sim 2.1$ mm), the particles will no longer be interrupted by the wall for both cases.

In summary, it was shown experimentally and numerically that the beam transport degrades in a configuration of a focusing planar wiggler with a superimposed axial uniform field, due to the cyclotron harmonics of the magnetoresonance even in the region of group I, as well as due to the spatial harmonics of the wigger field. The resonance also takes place in a helical wiggler with an axial field.

The authors are grateful to H. Oda for the coding support. Also, the authors would like to thank Dr. T. Nagashima, Dr. H. Maeda, Dr. K. Odajima, Dr. S. Shimamoto, and Dr. N. Shikazono for their encouragement.

[a]Permanent address: Faculty of Science, Saitama University, 255 Shimookubo, Urawa-shi, Saitama-ken, 338, Japan.
[b]Permanent address: Fukuoka Institute of Technology, Wajiro, Higashi-ku, Fukuoka, 811-02, Japan.

[1] T. J. Orzechowski *et al.*, Phys. Rev. Lett. **54**, 889 (1985).
[2] T. J. Orzechowski *et al.*, Phys. Rev. Lett. **57**, 2172 (1986).
[3] S. H. Gold, D. L. Hardesty, A. K. Kinkead, L. R. Barnett, and V. L. Granatstein, Phys. Rev. Lett. **52**, 1218 (1984).
[4] J. Fajans, G. Bekefi, Y. Z. Yin, and B. Lax, Phys. Fluids **28**, 1995 (1985).
[5] L. Friedland, Phys. Fluids **23**, 2376 (1980).
[6] R. K. Parker *et al.*, Phys. Rev. Lett. **48**, 238 (1982).
[7] R. M. Phillips, IRE Trans. Electron Devices **7**, 231 (1960).
[8] K. R. Chu and A. T. Lin, Phys. Rev. Lett. **67**, 3235 (1991).
[9] E. T. Scharlemann, J. Appl. Phys. **58**, 2154 (1985).
[10] K. Sakamoto, *et al.*, in *High Power Microwave Generation and Applications,* Proceedings of the International School of Plama Physics, edited by D. Akulina, E. Sindoni, and C. Wharton (Editrice Compositori, Bologna, Italy, 1992), p. 597.
[11] H. Diament, Phys. Rev. A **23**, 2537 (1981).